Climate Dynamics (2025) 63:143
https://doi.org/10.1007/s00382-025-07627-6

ORIGINAL ARTICLE

Multimodel GCM-RCM ensemble-based projections of tropical cyclone activities over CORDEX East Asia domain

Eunji Kim[1] · Taehyung Kim[1] · Taeho Mun[1] · Seok-Woo Shin[1] · Minkyu Lee[2] · Dong-Hyun Cha[1] · Eun-Chul Chang[3] · Joong-Bae Ahn[4] · Seung-Ki Min[5] · Jin-Uk Kim[6] · Young-Hwa Byun[6]

Received: 25 September 2024 / Accepted: 4 February 2025

Abstract
In this study, we investigated the future changes in tropical cyclone (TC) activities using regional climate models (RCMs) forced by multi-global climate models (GCMs). The simulation experiments were conducted at a 25-km horizontal resolution over the Coordinated Regional Climate Downscaling Experiment (CORDEX)-East Asia (EA) domain. The ensemble mean method was applied to reduce the uncertainty of each single RCM. During the historical period (1981–2005), the ensemble mean of RCMs captured TC frequency comparable to observation data but simulated their intensity weakly. When comparing the near future (2026–2050) and far future (2076–2100) periods under the high emission scenario to the historical period, the RCMs exhibited a consistent feature: the core region of TC genesis migrated northward. As the genesis region shifted, the TC activities also moved northward to the mid-latitude. In addition, the extreme intensity of landfalling TCs had increased above 25 °N compared to the historical period. These results are related to environmental fields; increasing relative vorticity and specific humidity of 850 hPa and weakening of vertical wind shear over the mid-latitude due to higher sea surface temperature compared to the historical period.

Keywords Tropical cyclone · CORDEX-EA · Future projection · Large-scale environments

1 Introduction

Since industrialization, the global mean temperature has increased by 1.0 °C due to the concentration of greenhouse gases, including carbon dioxide (IPCC 2021). The rising global temperature has the potential to induce significant changes in the frequency, intensity, and spatial distribution of extreme climate events (Allen et al., 2006; Coumou and Rahmstorf 2012; Otto et al. 2016; Stott et al. 2016). Consequently, numerous unprecedented extreme events have been witnessed across the world in recent years, including tropical cyclones (TCs). Coastal nations in the western North Pacific (WNP) are particularly susceptible to the impacts of TCs, as this area is the most frequent location for TC landfalls. The destructive potential of TCs is significant, and their associated risks and impacts are becoming increasingly severe (Park et al. 2015; Wang et al. 2016; Li et al. 2017; Choi et al. 2019; Kim et al. 2020). To mitigate casualties and economic damage, estimating future changes in TC characteristics is essential.

The global climate models (GCMs) are useful tools for analyzing TC characteristics and future projections.

✉ Dong-Hyun Cha
dhcha@unist.ac.kr

1 Department of Civil Urban Earth and Environmental Engineering, Ulsan National Institute of Science and Technology, 50, UNIST-gil, Ulju-gun, Ulsan 689-798, Republic of Korea

2 Renewable Energy Big Data Laboratory, Korea Institute of Energy Research, Daejeon, Republic of Korea

3 Department of Atmospheric Science, Kongju National University, Gongju, Republic of Korea

4 Department of Atmospheric Science, Pusan National University, Busan, Republic of Korea

5 Division of Environmental Science and Engineering, Pohang University of Science and Technology, Pohang, Republic of Korea

6 Climate Change Research Team, National Institute of Meteorological Sciences, Seogwipo, Republic of Korea

Published online: 28 February 2025

Previous studies have investigated the impact of global warming on TC activity using GCMs with various horizontal resolutions (Murakami and Wang 2010; Manganello et al. 2012; Strachan et al. 2013; Bacmeister et al. 2018; Bell et al. 2019; Chang et al. 2020; Roberts et al. 2020a; Hong et al. 2021). However, low-resolution GCMs could not simulate the structure of a TC well, and high-resolution GCMs required many computing resources. For more accurate simulations, regional climate models (RCMs) are used to research the characteristics of TCs as dynamical downscaling techniques (Knutson et al. 2008; Bender et al. 2010; Huang and Chan 2014; Tran et al. 2022). Also, several studies have used multi-model ensembles because a single RCM may have systematic errors (Torres-Alavez et al. 2021; Wu et al. 2022).

GCMs from the Coupled Model Intercomparison Project 5 and 6 (CMIP5 and CMIP6) (Taylor et al. 2012; Eyring et al. 2016), organized by the World Climate Research Programme (WCRP), are applied in the 5th and 6th Assessment Reports (AR5 and AR6) of the Intergovernmental Panel on Climate Change (IPCC), respectively. The future scenarios used in AR5 are Representative Concentration Pathway (RCP) scenarios, while AR6 uses Shared Socioeconomic Pathway (SSP) scenarios based on future socioeconomic changes and levels of mitigation and adaptation efforts. The Coordinated Regional Climate Downscaling Experiment (CORDEX), also initiated by the WCRP, is an international initiative facilitating the comparison and assessment of RCMs, generating a new set of climate change projections globally (Giorgi et al. 2009; Giorgi and Gutowski, 2015).

Numerous studies have been conducted within CORDEX-East Asia (EA), the regional branch of the CORDEX framework, aimed at predicting future changes in temperature and precipitation (Suh et al. 2012; Oh et al. 2013; Lee and Hong 2014; Zou et al. 2014; Gao et al. 2018; Kim et al. 2021a, b, 2023c; Giorgi et al. 2022; Seo et al. 2023; Tong et al. 2024). In addition, studies on TC activities over the WNP using the CORDEX-EA experiment are being actively conducted (Jin et al. 2016; Shen et al. 2017; Lee et al. 2019, 2020; Xi et al. 2021; Wu et al. 2022). Jin et al. (2016) evaluated TC activities over the WNP in five models [Hadley Centre Global Environmental Model version 3 regional climate model (HadGEM3-RA), Regional Climate Model (RegCM), Mesoscale Model version 5 (MM5), Weather Research and Forecasting model (WRF), and Global/Regional Integrated Model system (GRIMs)] with 50-km resolution included in the CORDEX-EA project. Shen et al. (2017) investigated the sensitivity of TC activity to the spectral nudging method and radiation schemes over the WNP basin in the WRF model. Lee et al. (2019) indicated that future changes and TC activity over the WNP under the RCP8.5 scenario were projected using four models (RegCM, MM5, WRF, and GRIMs) also participating in the CORDEX-EA project. However, these studies conducted TC analysis using low-resolution and a single large-scale forcing dataset. Moreover, there is still a lack of studies on TCs over the WNP in RCMs for RCP and SSP scenarios. Therefore, we need to use the results of CORDEX with a 25-km resolution to provide more reliable information and the ensemble of multi-GCMs.In this study, we investigated TC changes under future scenarios using 13 RCM simulations over CORDEX-EA and attempted to minimize uncertainty. This approach can provide more valuable information compared to previous studies.

This paper is organized as follows. Section 2 describes the information on RCMs, data, and tracking methods for TCs. Section 3 presents the evaluation of the climatological mean of TC activities for each RCM and the ensemble of RCMs in the historical simulation. Section 4 shows the projection of simulated TC activities and the associated environmental fields for future periods. Finally, Sect. 5 provides a summary and conclusion.

2 Data and methods

2.1 Models

In this study, we used RCMs [HadGEM3-RA, COSMO-CLM (CCLM), MM5, GRIMs, RegCM version 4.0 and 4.6 (RegCM4.0 and 4.6), and WRF] with 25-km horizontal resolution in CORDEX-EA phase 2 models. The configurations of the models are reported in Table 1. Four RCMs (HadGEM3-RA, CCLM, MM5, and RegCM4.0) are forced by HadGEM2-AO, which has a horizontal resolution of N96 (about 1.875° × 1.25°) with 38 vertical levels (Baek et al. 2013). Additionally, four RCMs (HadGEM3-RA, CCLM, MM5, and WRF) are forced by MPI-ESM-LR, which has T63 (1.875° × 1.865°) horizontal resolution and 47 vertical levels (Giorgetta et al. 2013). Five RCMs (HadGEM3-RA, CCLM, GRIMs, RegCM4.6, and WRF) are forced by UKESM with N96 (1.875° × 1.25°) and 85 vertical levels (Sellar et al. 2019). A spectral nudging technique is implemented in RCMs except HadGEM3-RA to diminish systematic errors in long-term simulations (von Storch et al. 2000; Cha et al. 2016; Moon et al. 2018). The analysis domain is set over the WNP including the EA region (10 °N – 45 °N, 100 °E – 155 °E) (Fig. 1).

Under the CORDEX-EA framework, the simulations cover the historical period of 1981–2005, 2026–2050 for the near future, and 2076–2100 for the far future under high emission scenarios: RCP8.5 for CMIP5-forced RCMs and SSP5-8.5 for CMIP6-forced RCMs. The RCP8.5 and SSP5-8.5 experiments represent the highest emission scenarios

Table 1 The configurations of 13 RCMs were forced by HadGEM2-AO, MPI-ESM-LR, and UK-ESM

	HadGEM2-AO				MPI-ESM-LR				UK-ESM				
	HadGEM3-RA	CCLM	MM5	RegCM4.0	HadGEM3-RA	CCLM	MM5	WRF	HadGEM3-RA	CCLM	GRIMs	RegCM4.6	WRF
Horizontal Resolution	25-km				25-km				25-km				
Vertical Layers	63 eta	40 hybrid	24 sigma	23 sigma	63 eta	40 hybrid	24 sigma	30 eta	63 eta	40 hybrid	28 sigma	23 sigma	30 eta
Microphysics	single moment bulk	Seifert and Beheng	Reisner2	SUBEX	single moment bulk	Seifert and Beheng	Reisner2	WSM3	single moment bulk	Seifert and Beheng	WSM1	SUBEX	WSM3
Cumulus Parameterization	Revised mass flux	Tiedtke	Kain-Fritch	Emanuel	Revised mass flux	Tiedtke	Kain-Fritch	BMJ	Revised mass flux	Tiedtke	SAS	Emanuel	BMJ
Radiation	General2	Ritter and Geleyn	CCM2	CCM3	General2	Ritter and Geleyn	CCM2	CAM	General2	Ritter and Geleyn	Chou et al.	CCM3	CAM
Planetary Boundary Layer	MOSES-II	Davies and Turner	YSU	Holtslag	MOSES-II	Davies and Turner	YSU	YSU	MOSES-II	Davies and Turner	YSU	Holtslag	YSU
Land Surface	JULES	TERRA ML	CLM3	CLM3.5	JULES	TERRA ML	CLM3	Noah	JULES	TERRA ML	Noah	CLM4.5	Noah
Spectral Nudging	No	Yes	Yes	Yes	No	Yes	Yes	Yes	No	Yes	Yes	Yes	Yes
Simulation Period	Historical: 1979–2005 Future (RCP8.5): 2006–2100				Historical: 1979–2005 Future (RCP8.5): 2006–2100				Historical: 1979–2014 Future (SSP5-8.5): 2015–2100				

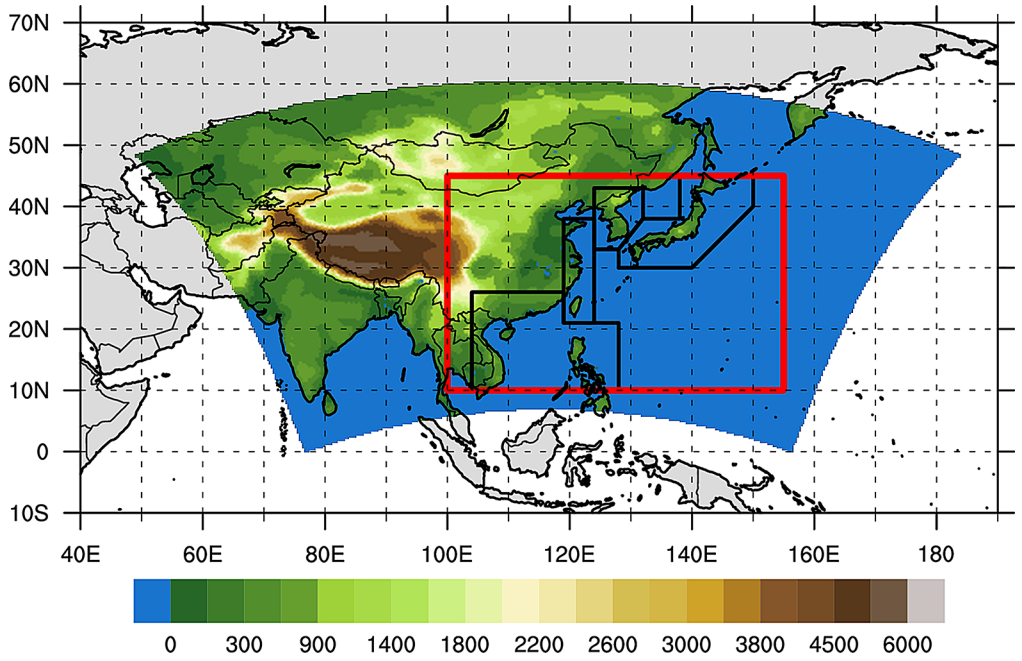

Fig. 1 CORDEX-East Asia Phase 2 domain and topography (shading, m). The red boxed area indicates the analysis region used in this study. The black boxed areas represent the South China and Philippines (SCP), East China and Taiwan (ECT), Korea (KOR), and Japan (JPN) regions, listed in order from left to right

and are selected to estimate the potential response of TC activity to maximum warming.

2.2 Data

The best track data used in this study was obtained from the Regional Specialized Meteorological Centers (RSMC) Tokyo-Typhoon Center to evaluate simulated TC activities. This dataset includes TC location every 6 h, maximum wind speed, minimum sea level pressure of the TC center, etc. TCs categorized as tropical storms or stronger (wind speed greater than 17 m s^{-1}) were analyzed. We focused on the season from June to November (JJASON), when TCs frequently form over the WNP region. ERA5 reanalysis data (Hersbach et al. 2020) was used to compare the simulation of atmospheric fields of models from 1981 to 2005 for the historical period.

2.3 Methods

The tracking and detection methods of TCs in this study are similar to those in previous studies (Cha et al. 2011; Jin et al. 2016; Lee et al. 2020; Kim et al. 2023b). The tracking methods were as follows: (1) the potential storm is a local minimum of sea level pressure within the 500 km radius; (2) the maximum surface wind exceeds the wind speed threshold within the 500 km radius; (3) the maximum relative vorticity at 850 hPa exceeds the vorticity threshold within the 500 km radius; (4) the sum of the temperature deviations at 300, 500, and 700 hPa exceeds the temperature anomaly threshold within the 500 km radius; (5) the maximum wind speed at 850 hPa is larger than that at 300 hPa within the 500 km radius; (6) the duration is not shorter than 2 d; (7) tracks are traced from these identified potential storms. Thresholds for each model were determined through sensitivity tests (see Table 2). The goal of this study is not to compare the performances of the models but to create an optimal ensemble of TC activity over the WNP with reduced uncertainty, therefore we apply different thresholds for each model to detect TCs.

To reduce the uncertainty associated with a single RCM, we applied the equal weighting ensemble averaging (EWA) method to 13 RCMs. The ensemble mean of these 13 models is hereafter referred to as ENS.

Table 2 The threshold for tracking TCs of each RCM

		Wind speed (m s^{-1})	Vorticity (10^{-5} s^{-1})	Temperature (K)
CMIP5	HadGEM3-RA	14.0	5.0	1.0
	CCLM	15.0	7.0	2.0
	SNU-MM5	17.0	12.0	3.5
	RegCM4.0	15.0	7.0	2.0
	WRF	14.0	5.0	1.0
CMIP6	HadGEM3-RA	14.0	5.0	1.0
	CCLM	15.0	7.0	2.0
	GRIMs	17.0	12.0	3.5
	RegCM4.6	14.0	5.0	1.0
	WRF	14.0	5.0	1.0

We calculated the genesis and track density for each 2.5° x 2.5° grid using RSMC best track data and outputs from the 13 RCMs. Additionally, synoptic variables from ERA5 reanalysis data and the outputs from the 13 RCMs were converted to 0.25° x 0.25° grids. For evaluation with the model ensemble and ERA5, environmental variables were also converted to the grids of ERA5. When a TC moved within the same grid point, the genesis and track density were computed only once. We defined the genesis and track positions of observed TCs originating outside the analysis domain as the first and subsequent positions after entering the boundaries of the analysis domain.

3 Evaluation of TC simulation skill in the historical period

3.1 Evaluation for 13 RCMs

Before analyzing TCs in future periods, the spatial distribution of TCs in the historical periods was compared with observation data to evaluate the TC simulation performance of RCMs. Figure 2 depicts the genesis density of TCs for 13 RCMs and RSMC best track data during the historical period. Three core regions of TC genesis were observed in the best track data: the South China Sea (SCS), the Philippine Sea (PS), and the Mariana Trench area (MT) (Fig. 2a). The 13 RCMs exhibited different characteristics in simulating TCs. HG2_HG3RA did not capture the central region over the PS and overestimated over the SCS. HG2_CCLM reproduced the core region over the PS northerly but showed an overestimation over the SCS, showing the lowest spatial correlation coefficient among the models. HG2_MM5 overestimated genesis density over the core regions. In addition, the central region in the PS was shifted northeastward. HG2_RegCM4.0 simulated a distribution similar to HG2_HG3RA. MPI_HG3RA reproduced four core regions and showed higher densities compared to RSMC data; however, it exhibited a high spatial correlation coefficient. In MPI_CCLM, the genesis region over the PS (SCS and ES) was simulated widely (reasonably), but the frequency was similar (overestimated). MPI_MM5 overestimated TC genesis between 10 °N − 20 °N. MPI_WRF underestimated genesis over the PS and overestimated it over the SCS and

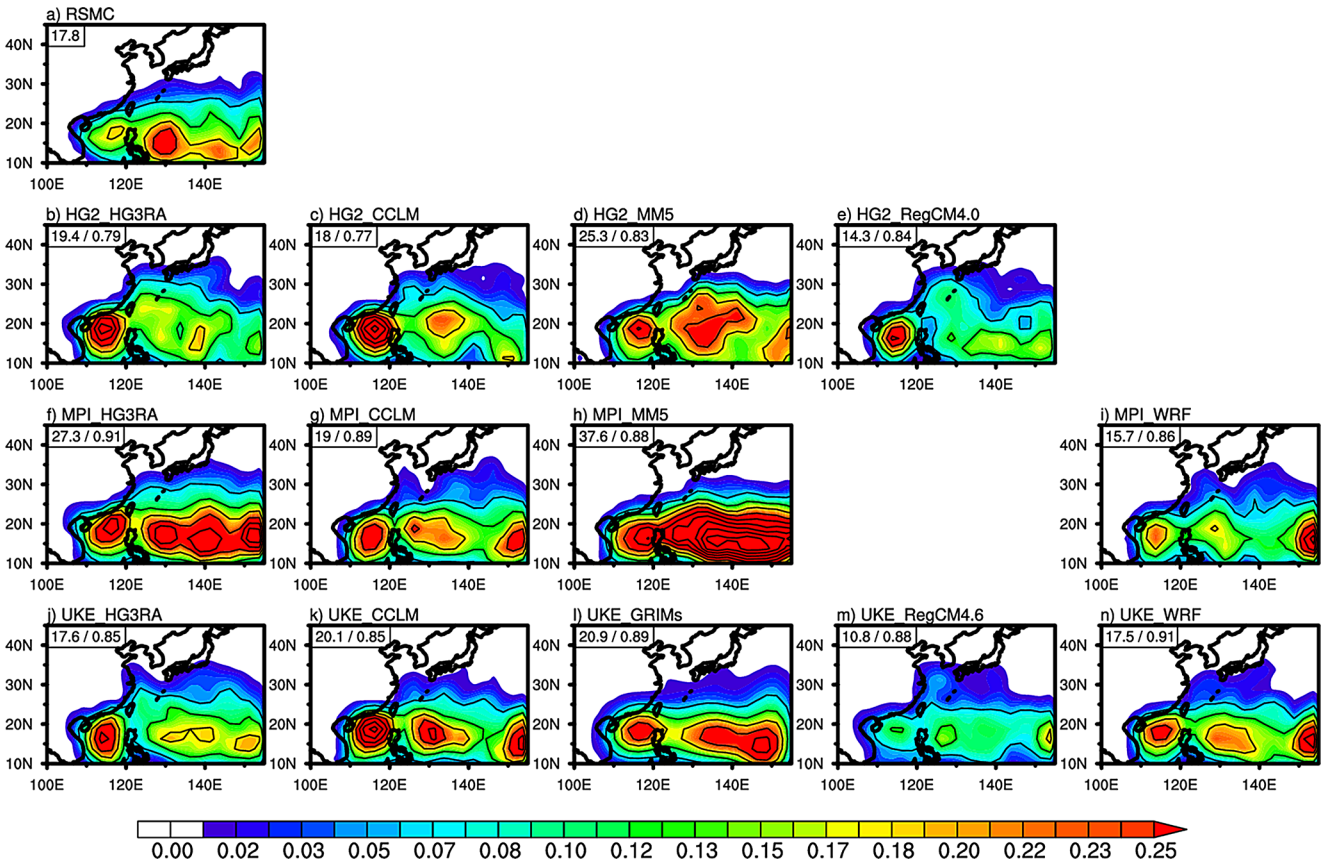

Fig. 2 Climatological mean of TC genesis density from (**a**) RSMC and historical run of (**b**) HadGEM3-RA, (**c**) CCLM, (**d**) MM5, (**e**) RegCM4.0 forced by HadGEM2-AO, and (**f**) HadGEM3-RA, (**g**) CCLM, (**h**) MM5, (**i**) WRF forced by MPI-ESM-LR, and (**j**) HadGEM3-RA, (**k**) CCLM, (**l**) GRIMs, (**m**) RegCM4.6, and (**n**) WRF forced by UK-ESM for 25 years (1981–2005). The values in each panel indicate the mean number of TCs (NTC) and spatial correlation coefficient

MT simulating the largest number of TCs among the models. UKE_HG3RA showed a high density of TCs in the SCS but could not capture the core region of TCs in the eastern Philippines. UKE_CCLM exhibited a higher genesis density of TCs over the eastern Philippines. UKE_GRIMs exhibited an overestimation of genesis density due to the use of WSM1, a Micro Physics Scheme (MPS) known for simulating more TCs (Kim et al. 2017). UKE_RegCM4.6 simulated a lower frequency of TC genesis, reproducing the smallest number of TCs among the models. According to Lagare et al. (2022), the low frequency of TCs in RegCM is attributed to the use of the Holtslag Planetary Boundary Layer (PBL) parameterization scheme, which tends to simulate fewer TCs. UKE_WRF moderately simulated TC core regions, showing high density in the SCS and MT with a number of TCs most similar to observations and the highest correlation coefficient alongside MPI_HG3RA. Although using the same GCM, differences in TC simulation across RCMs were evident.

Figure 3 compares the mean number of TCs (NTC) with the mean maximum wind speed (MWS) for 25 years. For NTCs, there were differences between RCMs with different forcings. Among the three GCMs, the UK-ESM simulated the fewest TCs, HadGEM2-AO showed a moderate number, and MPI-ESM-LR simulated the highest number. Additionally, CCLM and HG3RA, which incorporated all three forcings, showed a nearly identical simulation of NTC across the RCMs. Similarly, WRF, which incorporated two forcings, exhibited comparable results. These suggest a significant dependency on the GCM and RCM forcings in the simulation of NTC. The MWS average for each GCM tended to be significantly affected by specific RCMs (e.g., MM5 and GRIMs) to overestimate the TC counts. Overall, RCMs such as CCLM, HG3RA, WRF, and MM5 demonstrated similar mean MWS, indicating a considerable RCM dependency in the simulation of TC intensity.

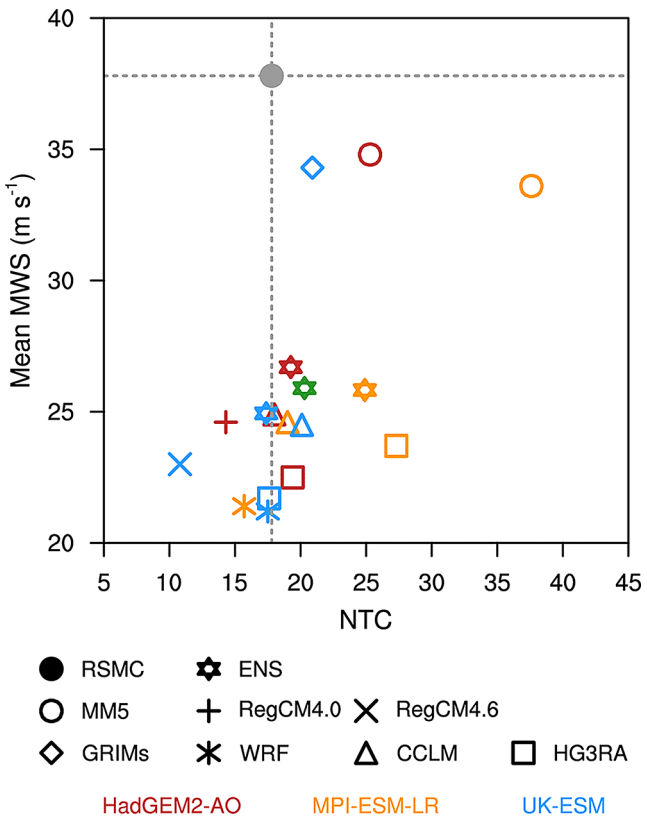

Fig. 3 Relationship between the mean NTC (yr^{-1}) and mean maximum wind speed (MWS, m s^{-1} yr^{-1}). The colors represent the GCMs, and the symbols denote the RCMs

Figure 4 shows the track density of TCs in the 13 RCMs. In the observational data, the main activity region appeared near the Philippines (Fig. 4a). Similar to the TC genesis density, MPI_MM5 overestimated TC track density, while UKE_RegCM4.6 underestimated it. Other RCMs also exhibited track density distributions based on genesis density. In terms of the spatial correlation coefficient, unlike the genesis density, all models showed high correlation, with MPI_HG3RA and UKE_HG3RA exhibiting the highest values. Despite being forced by the same GCM and applying nudging techniques, each RCM yielded different results and systematic biases. This diversity in simulation results highlights the need for ensemble approaches.

3.2 Ensemble mean results

The genesis and track density of TCs in the 13 RCMs were analyzed using the ensemble method (Fig. 5). The results indicated that the ENS was mainly simulated over the SCS, PS, and MT (Fig. 5b) and exhibited more TC genesis over the SCS and MT, and less in the east of the Philippines compared to the observation data (Fig. 5c). The ENS reproduced TC activity centered over the SCS and around 125 °E – 145 °E (Fig. 5e). In addition, ENS underestimated TC activities towards the Korean Peninsula and Japan, but overestimated TC activities in the SCS and MT (Fig. 5f), consistent with findings from previous studies (Lee et al. 2019). There was little difference in NTC compared to RSMC (Table 3, Difference: +2.5). However, mean intensity (MWS and minimum sea level pressure (MSLP) was noticeably underestimated, and the duration was shorter in the ENS. The shorter duration can be associated with the underestimated activities of TCs migrating to mid-latitude. Nevertheless, the distributions of TC genesis and tracks in the ENS (with spatial correlations of 0.92 and 0.95, respectively) show reasonable agreement with RSMC compared to the individual RCMs included in the ENS (with correlations ranging from 0.77 to 0.91 and 0.87 to 0.95).

To evaluate the intensity of TCs in the ENS compared to observational data, we analyzed the distribution of TCs

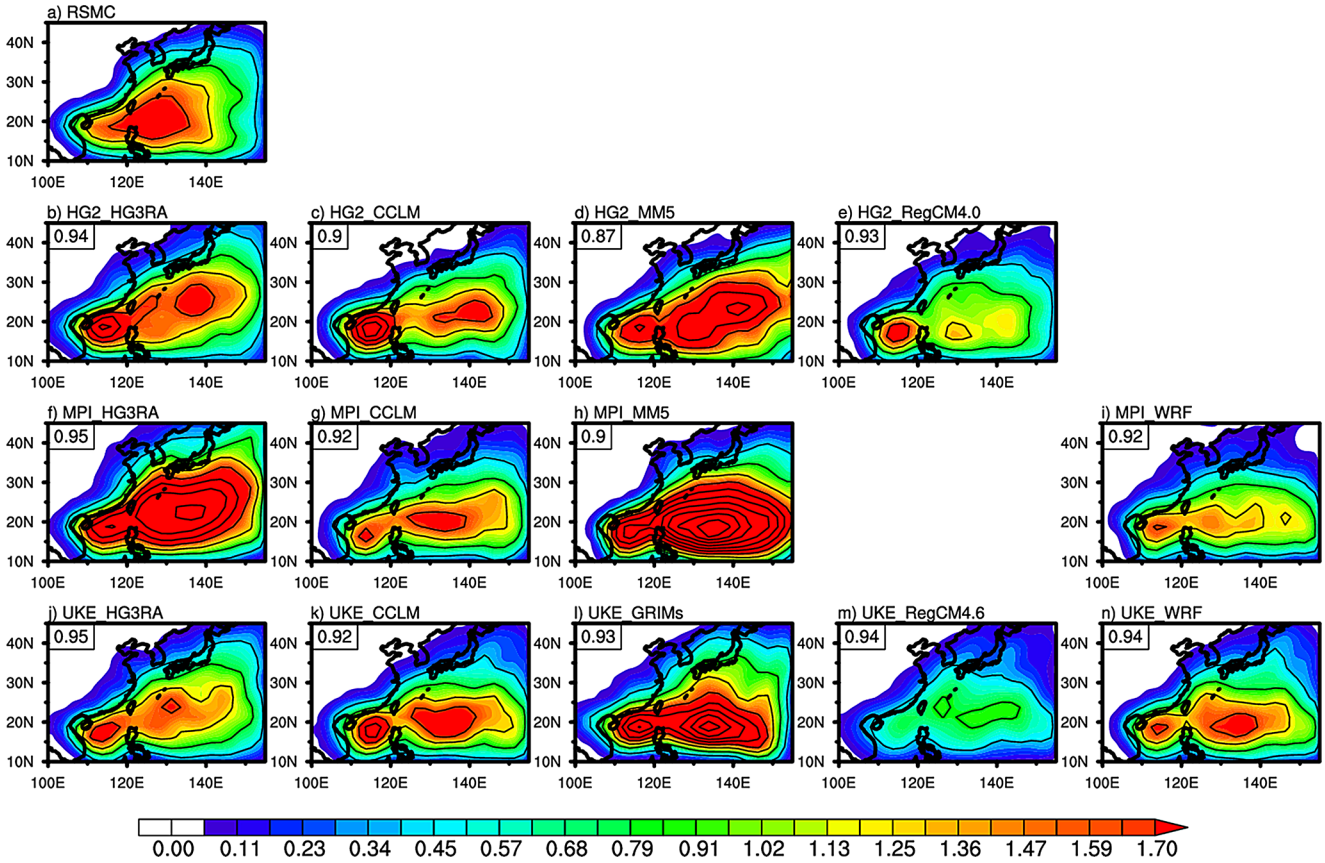

Fig. 4 As in Fig. 2, but for TC track density. The value in each panel indicates the spatial correlation coefficient

by category (Fig. 6). The results indicated that some RCMs tended to overestimate the maximum TC intensity. On average, the number of simulated TCs was comparable across RCMs. However, TCs in the tropical storm (TS) category were simulated more frequently than observed, with an average of 9.1 in the ENS compared to 2.2 in observations. For the severe tropical storm (STS) category, the simulated and observed values were 6.8 and 3.7, respectively. Conversely, the typhoon (TY) category revealed that the ENS simulated significantly fewer TCs than observed, as most models struggled to accurately represent strong TCs (ENS: 3.8, RSMC: 11.8). The maximum intensity in the ENS was higher than that observed, primarily due to the MPI_MM5 model's tendency to simulate stronger TCs on average. Thus, RCMs generally overestimated the frequency of weaker TCs while underestimating the frequency of stronger TCs. Although TC frequency was simulated with reasonable accuracy, the challenge of simulating strong TY-category TCs at a 25-km resolution is evident. This limitation is attributed to the inability of coarse resolution models to realistically capture TC dynamics (Cha et al. 2011; Jin et al. 2016; Roberts et al. 2020b; Li et al. 2021; Kim et al. 2023a).

The cause of TC simulation in ENS was identified through the analysis of the environmental fields associated with TCs. Figure 7 shows the mean field from ERA5 (left panels) and the historical run of ENS, and the differences between the ENS simulations and ERA5 (right panels). At 850 hPa, positive (negative) relative vorticity was shown below (above) 20 °N, with a pattern of decreasing specific humidity from low to mid-latitude in ERA5 reanalysis data (Fig. 7a and d). There was an anticyclonic circulation over the WNP, with southwesterly winds distributed over the Korean Peninsula and South of Japan. Additionally, in the observation, TCs were primarily generated around the monsoon trough area. Sea surface temperature (SST) showed a decreasing pattern from low to mid-latitude, with little vertical wind shear (VWS) as the barotropic atmosphere at low-latitude and a strong distribution at mid-latitude where it is baroclinic, particularly around 30 °N−40 °N (Fig. 7g and j). After formation, TCs move along the western boundary of the western North Pacific Subtropical High (WNPSH) (Kim et al. 2012). WNPSH is typically defined by the 5880-gpm line (He et al. 2015; Yoon et al. 2018; Mun et al. 2024), and in the observations, TC movement occurred along this line (Figs. 5d and 7g). The ENS simulated high positive relative vorticity below 20 °N and positive vorticity biases at

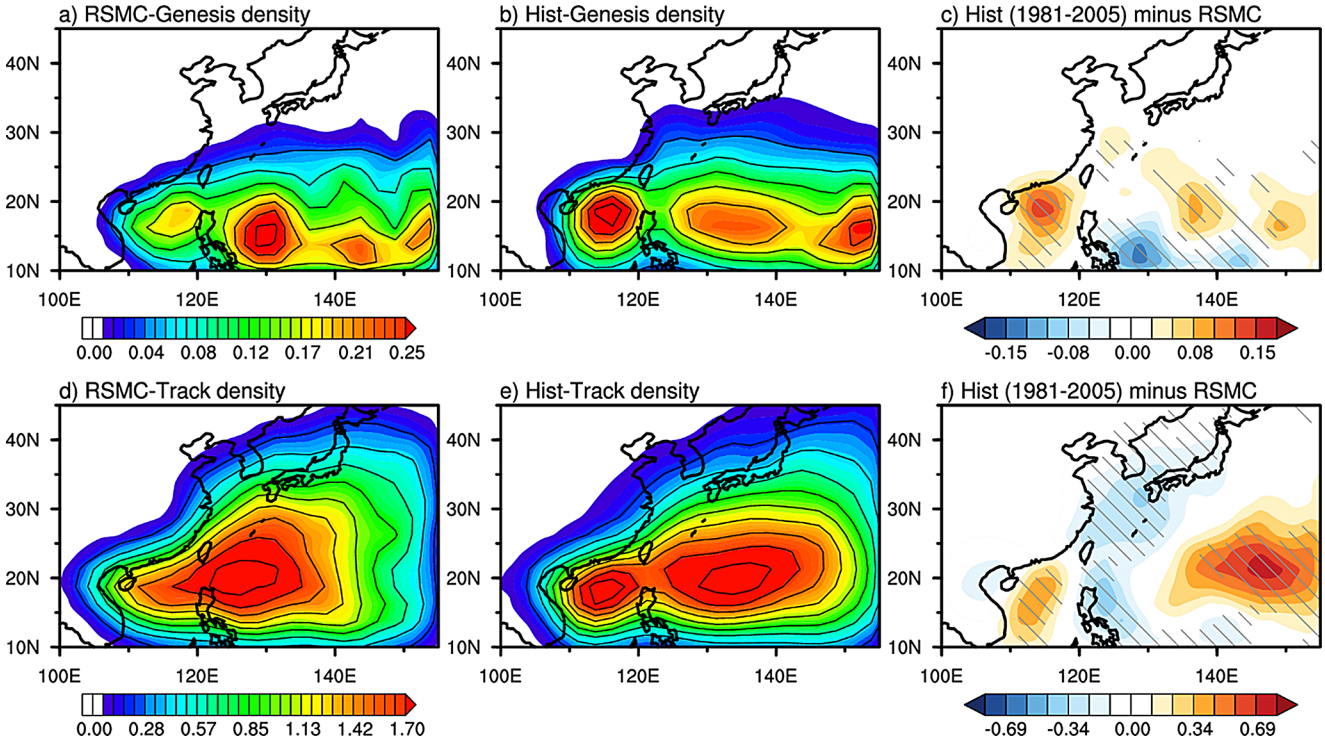

Fig. 5 The climatological mean of TC genesis density and track density from (**a, d**) RSMC and (**b, e**) historical run of ENS, respectively. Differences between ENS and RSMC (**c**) TC genesis density and (**f**) track density for 25 years (1981–2005). Backslashes denote the consistency between RCMs indicating 10 RCMs have the same signal

Table 3 Statistics for the mean NTC, mean intensity, and duration of TC during the historical, near, and far future period (1981–2005, 2026–2050, and 2076–2100). Changes between the model results that are statistically significant at the 95% confidence level using a two-sided Student's t test are shown in boldface

	RSMC 1981–2005	Historical 1981–2005	Difference (Hist. - RSMC)	High emission scenario		Change (Future - Hist.)	
				2026–2050	2076–2100	2026–2050	2076–2100
NTC (yr^{-1})	17.8	20.3	+2.5	19.7	17.0	−0.6 (−3.0%)	−3.3 (−16.3%)
MWS ($m\ s^{-1}yr^{-1}$)	37.8	25.9	−11.9	25.9	26.6	0 (0%)	+0.7 (+2.7%)
Minimum Sea-level pressure ($hPa\ yr^{-1}$)	956.6	984.0	+27.4	984.1	983.2	+0.1 (0%)	−0.8 (−0.1%)
Duration ($hr\ NTC^{-1}yr^{-1}$)	133.4	118.2	−15.2	118.7	113.9	+0.5 (+0.4%)	−4.3 (−3.6%)

850 hPa between 10 °N and 30 °N, in particular SCS compared to the reanalysis data (Fig. 7b and c). This distribution contributed to the development of TCs at these locations, with an overestimated frequency of TCs where the lower-level vorticity increased compared to ERA5 (Fig. 5c). Figure 7d shows the specific humidity and wind of 850 hPa in the ENS of the historical period. It depicted the highest water vapor below 25 °N during the historical period, with a decrease toward mid-latitude. The wind field exhibited cyclonic circulation over the SCS and PS, with southeasterly winds prevailing over the MT. Specific humidity showed little difference between the ENS and ERA5 over the ocean, with drier features over the Korean Peninsula and China. The monsoon trough was strengthened by a strong westerly bias at low-latitude, and wind fields exhibited a weakening of the anticyclonic circulation over the SCS and WNP (Fig. 7f). These stronger bias of monsoon trough and weaker bias of circulation may induce a positive relative vorticity bias, promoting increased TC genesis over the SCS and MT. Moreover, a northeasterly bias over the East China Sea (ECS) could diminish TC activity towards the Korean Peninsula and Japan (Fig. 5e). ENS showed negative SST biases over the PS and MT, which are major TC activity regions, with positive biases over the coastal areas of Korea, Japan, and China (Fig. 7i). Due to the negative SST bias in ENS, TCs may not get as much energy as observed, resulting in underestimated intensity (Table 3). Additionally, the overestimation of TC genesis and activity in the MT region

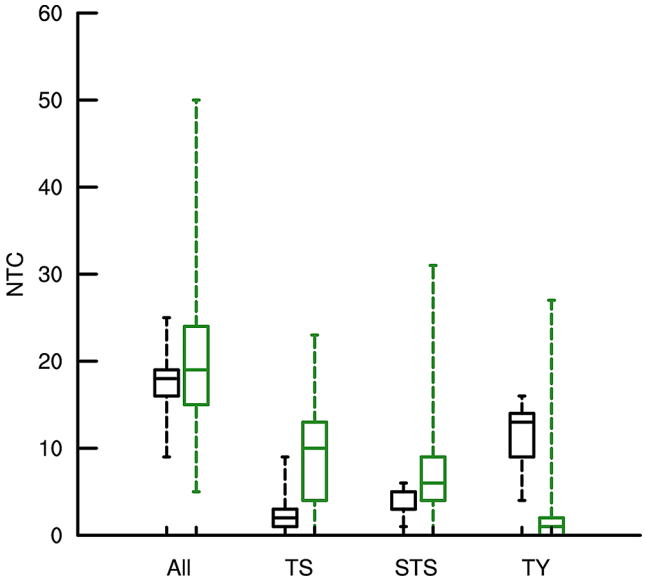

Fig. 6 The box plot in the historical period (1981–2005) of the number of all TCs, tropical storm (TS), severe tropical storm (STS), and typhoon (TY) averaged by year. Black boxes indicate the RSMC best track data, while green boxes represent all 13 RCMs, not the ensemble mean. The center line denotes the median, box limits denote the lower and upper quartiles, and whiskers denote the minimum and maximum. ($17 \leq TS < 25$, $25 \leq STS < 33$, $TY \geq 33$ m s^{-1})

compared to the observation may be linked to the intensified cyclonic circulation due to the weakening of the WNPSH. VWS showed a more dominant distribution across the domain compared to ERA5, except for the area around 20 °N, 100 °E − 120 °E (Fig. 7l). This positive bias of VWS in most TC activity regions may explain the underestimation of TC intensity, similar to SST. The differences compared to ERA5 may result from systematic biases associated with the characteristics or physical parameterization schemes of each RCM, or from the driving GCM. In this study, most models, except for HG3RA, employed spectral nudging, and SSTs were directly provided by the GCMs. This suggests that the biases are primarily attributable to the GCMs, as supported by several previous studies (Gao et al. 2012; Park et al. 2016; Lee et al. 2019).

4 Future changes in the TC activities

In this section, we analyze the changes in TC activity by comparing the results between historical period and future periods and investigate the causes of the changes. Firstly, we examined the future changes in TC genesis and track density (Fig. 8). Figure 8a indicates the difference in simulated TC genesis density between the ENS of near future and historical periods. The difference showed that the TC genesis tended to decrease below 20 °N and increase significantly over the northwestern part of the SCS and the ECS in the near future. The far future exhibited a similar pattern to the near future but with a larger absolute value (Fig. 8b). 75% among 13 RCMs simulated a significantly decreasing TC genesis in low-latitude. In the near future, the high-emission scenarios experiment predicted a decrease in TC activity from the SCS to PS compared to the historical experiment. In contrast, TC activity increased over the south of Japan and the Korean Peninsula (Fig. 8c). The far future period showed a significant decrease in TC activity below about 30 °N and an increase in activity over the east of Japan above 30 °N (Fig. 8d). These results were consistent with previous studies (Bacmeister et al. 2018; Bell et al. 2019; Roberts et al. 2020a; Chang et al. 2020; Fu et al. 2023). Comparing the NTC between the historical and the future experiment, there was a decrease in NTC in both the near and far future, approximately −3.0% and −16.3% respectively, with the decrease being more notable in the far future (Table 3). MWS remained unchanged in the near future and increased in the far future. MSLP increased slightly in the near future and decreased in the far future. The duration did not change in the near future (+0.4%), while it slightly decreased in the far future (-3.6%). The increase in duration in the near future was 0.5 h per TC, which is almost unchanged. This was due to increased TC activity from the south of Japan to the Korean Peninsula, which could have maintained the total duration even as the TC genesis and activity decreased below 20 °N (Fig. 8b and e). In the far future, the duration decreased by 4.3 h per TC, as the occurrence and activity of TCs decreased significantly from 10 °N to 20 °N (Fig. 8c and f). In summary, the NTC will decrease in both the near and far future under high emission scenarios, but TC activity is expected to be more concentrated in the mid-latitude in the near future. Conversely, in the far future, NTC is expected to decrease, and their duration is projected to be shorter; however, TCs are anticipated to exhibit increased intensity.

Additionally, we analyzed the intensities of TCs by category (Fig. 9). As detailed in Table 3, both the near and far future periods projected fewer total TCs on average compared to the historical period, with a more pronounced reduction in the far future. Specifically, the mean NTC were 9.1, 8.3, and 6.8 for the TS category, and 6.8, 6.6, and 5.7 for the STS category in the historical, near future, and far future periods, respectively, with the smallest maximum values in the far future. Conversely, for the TY category, mean NTC were 3.8, 4.2, and 4.2, indicating a slight increase in future periods compared to the historical period. In particular, the maximum values were 27, 30, and 36, with the largest value in the far future. These results suggest a potential for more intense TCs in the far future compared to both the historical and near future periods.

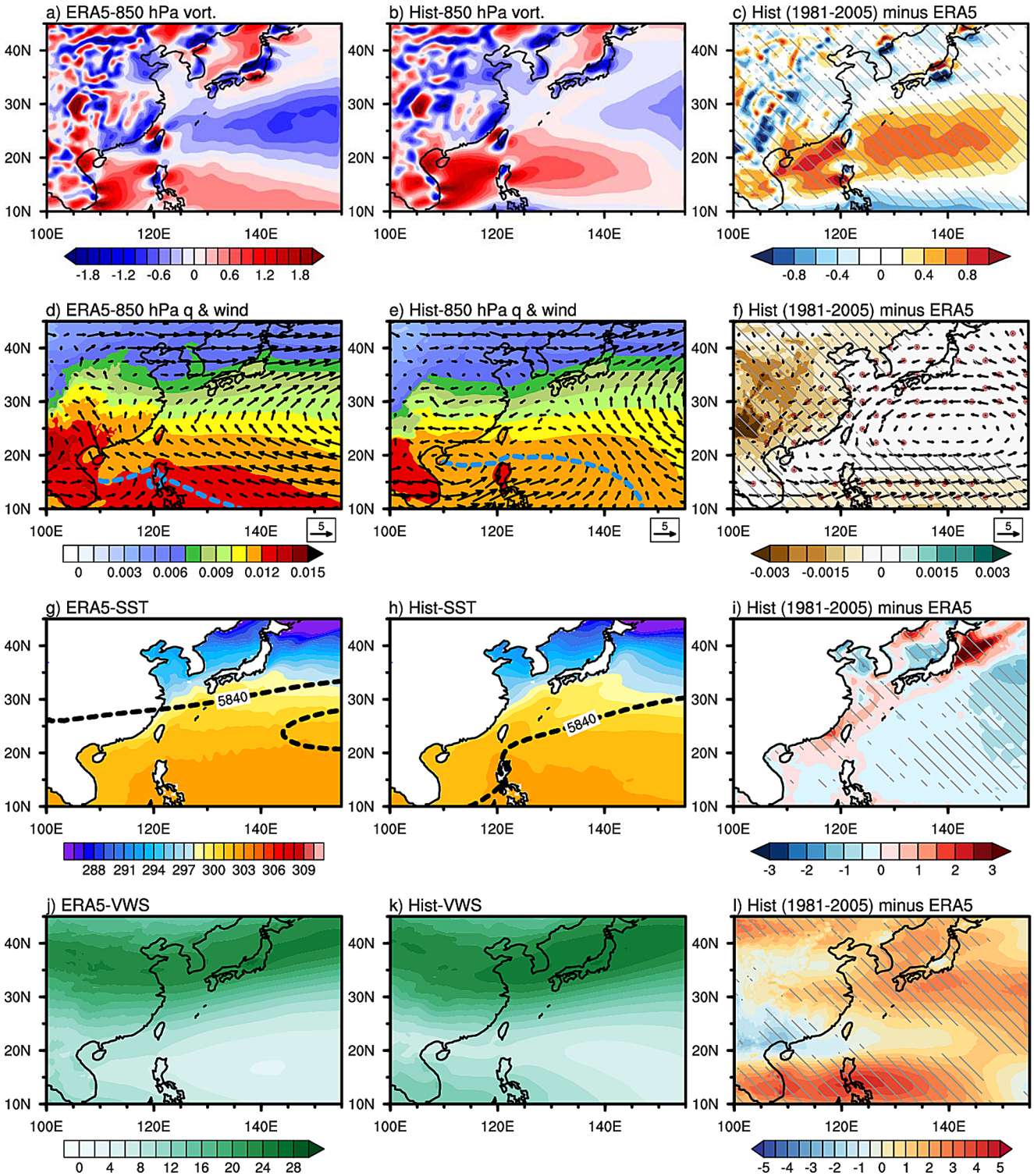

Fig. 7 (**a-c**) Relative vorticity at 850 hPa (10^{-5} s^{-1}); (**d-f**) specific humidity (shading, kg kg^{-1}), wind (vectors, m s^{-1}) at 850 hPa, and the monsoon trough (blue dashed line); (**g-i**) sea surface temperature (**K**) and geopotential height at 500 hPa with 5840 and 5880 gpm (black dashed line); and (**j-l**) vertical wind shear (m s^{-1}) from June to November. Panels show the climatological mean for (left) ERA5, (middle) the historical run of ENS, and (right) the difference between ENS and ERA5 for 25 years (1981–2005). Backslashes and red dots denote the consistency between RCMs indicating 10 RCMs have the same signal

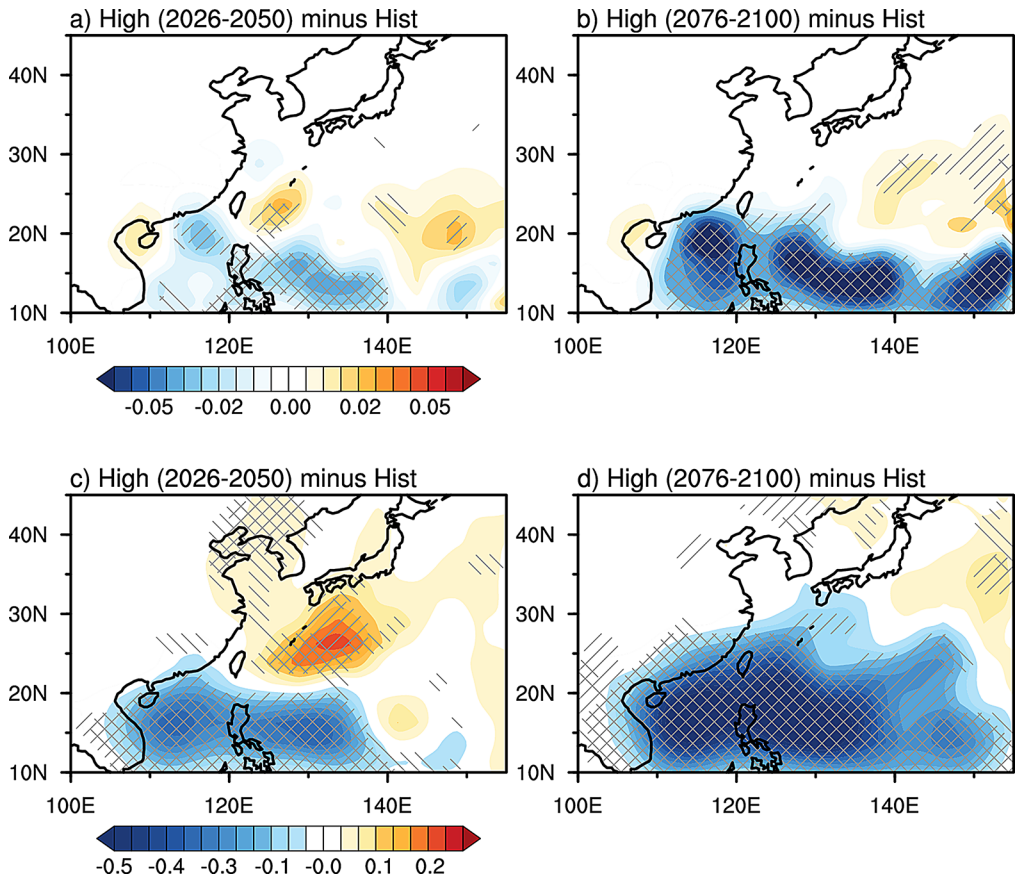

Fig. 8 (**a-b**) TC genesis density and (**c-d**) TC track density for the differences between high emission scenarios for the near future (2026–2050) and far future (2076–2100) and historical run (1981–2005). Slashes indicate significance at the 90% confidence level based on the Student's t-test. Backslashes denote the consistency between RCMs indicating that 10 RCMs have the same signal. Hatched lines indicate both

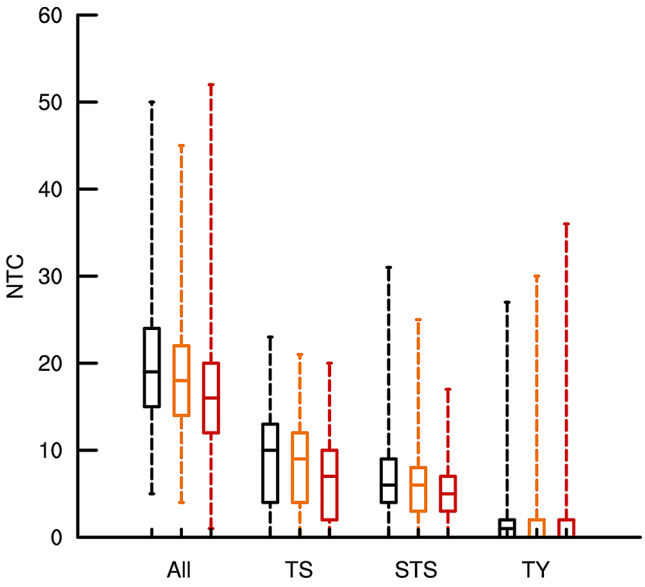

Fig. 9 As in Fig. 5, but for ENS run. Black boxes indicate historical run, orange boxes indicate a high emission scenario of the near future (2026–2050), and red boxes indicate a high emission scenario of the far future (2076–2100)

To analyze landfalling TCs, we examined the information on first-landfall points (Fig. 10). In the historical period, 7.4 TCs per year made landfall in the EA region. In the near future, 6.9 TCs per year, and in the far future, 5.6 TCs per year made landfall, respectively. The ratio of landfalling TCs (the number of landfalling TCs over the number of genesis TCs) decreased in both future periods compared to the historical period (near future: -1.2%, far future: -3.1%). The reduced number of landfalls projected for future periods is due to the decreased TC genesis compared to the historical period (see Table 3). However, the wind speed at landfall increased in the future, with the far future showing a greater increase than the near future (near future: +0.8%, far future: +2.5%). This means that fewer but stronger TCs are more likely to make landfall. In addition, when analyzing the number of landfalling TCs by region, the Korea (KOR), Japan (JPN), and East China and Taiwan (ECT) regions showed an increase in landfall frequency in the near future due to enhanced TC activity around 20 °N. However, in the far future, TC activity decreased overall, leading to a reduction in landfalling TCs. The South China and Philippine (SCP)

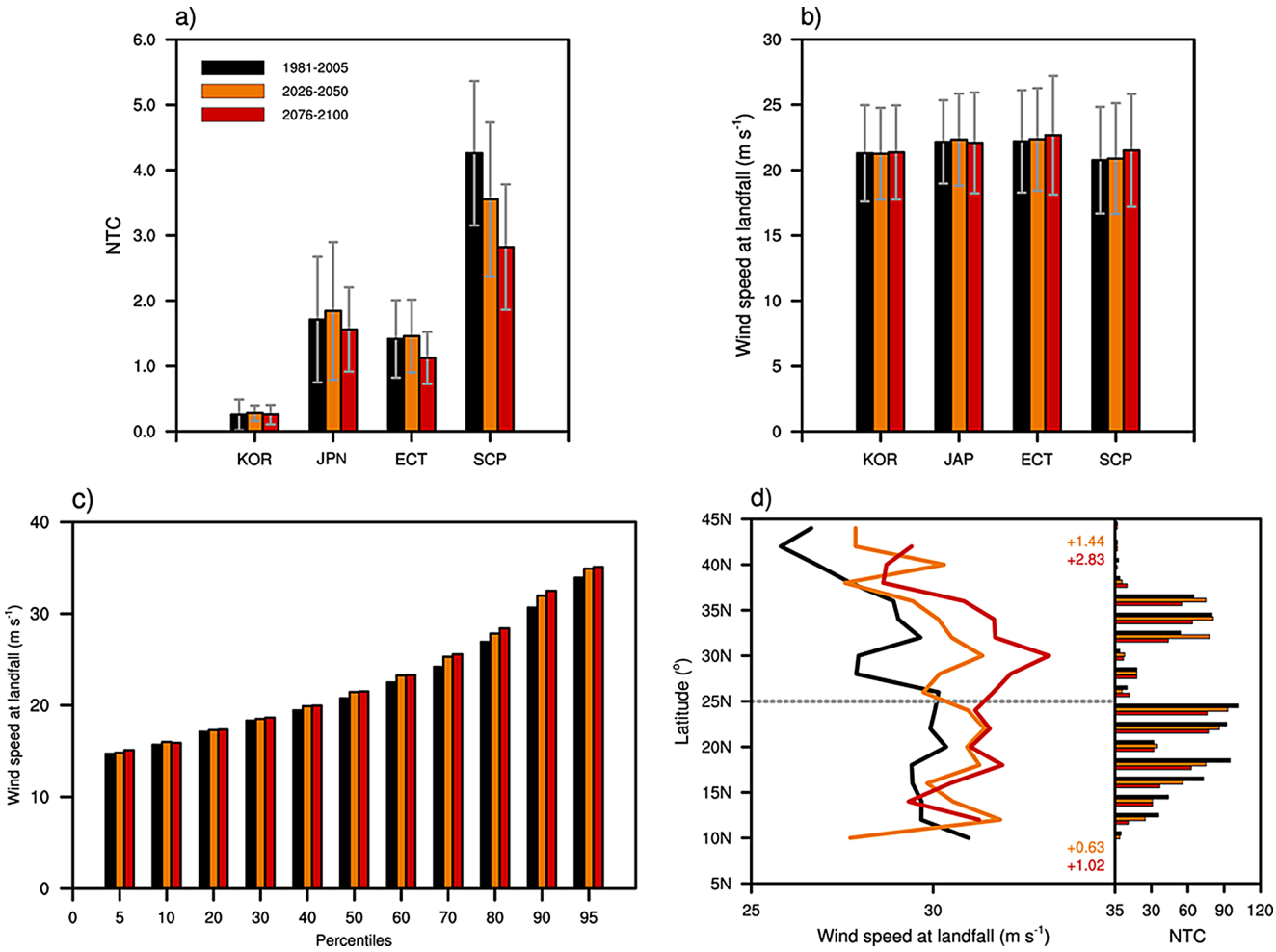

Fig. 10 (**a**) Mean NTC (yr^{-1}) and (**b**) MWS ($m\ s^{-1}\ yr^{-1}$) at landfall in East Asia regions during the historical, near, and far future period (1981–2005, 2026–2050, and 2076–2100). Locations of East Asia regions are provided in Fig. 1. (**c**) Percentiles of wind speed at landfall. (**d**) Wind speeds at landfall exceeding the 70th percentile, presented by latitude. The bar graph indicates the NTC at landfall for all 13 RCMs at each latitude, with latitude values averaged every 2°. The orange bars and lines represent the near future period (2026–2050), while the red bars and lines denote the far future period (2076–2100). Orange (Red) text indicates the differences between the near (far) future and the historical period. The whisker in (**a**) and (**b**) indicate one standard deviation of the 13 RCMs

region, located in the 10 °N –20 °N, simulated a gradual decrease in TC activity over time, resulting in a reduction in landfalling TCs as well (Fig. 8a and b, and Fig. 10a). Wind speed showed little variation in the KOR region across all three periods, while in JPN, the mean wind speed of landfalling TCs slightly increased in the near future. In contrast, in ECT and SCP, the wind speed increased progressively in the far future (Fig. 10b). We further examined the percentiles for wind speed at landfall (Fig. 10c). Differences in wind speeds between the near future and far future scenarios began to emerge from the 70th percentile. Therefore, wind speeds exceeding the 70th percentile were analyzed according to latitude (Fig. 10d). Below 25 °N, the wind speeds for historical, near future, and far future scenarios were relatively similar, with near future values at +0.6 m s^{-1} (+2.1%) and far future values at +1.0 m s^{-1} (+3.4%). In contrast, above 25 °N, a notable difference between the near future and far future scenarios compared to historical values was observed, with near future wind speeds at +1.4 m s^{-1} (+5.1%) and far future wind speeds at +2.8 m s^{-1} (+10.1%). 25 °N serves as a dividing line between TCs that moved westward to the SCS and those that recurved northward. The analysis of TCs making landfall above 25 °N suggests that there is a higher likelihood of stronger TCs making landfall in central China, northern China, Korea, and Japan, in the far future compared to the historical period.

An analysis of the environmental field associated with TC was conducted to examine the causes of the changes in TC activities in the future (Fig. 11). Compared to the historical period, the near future period simulated positive relative vorticity anomalies in 20 °*N* −30 °N (Fig. 11a). Similarly, the difference between the far future and the historical

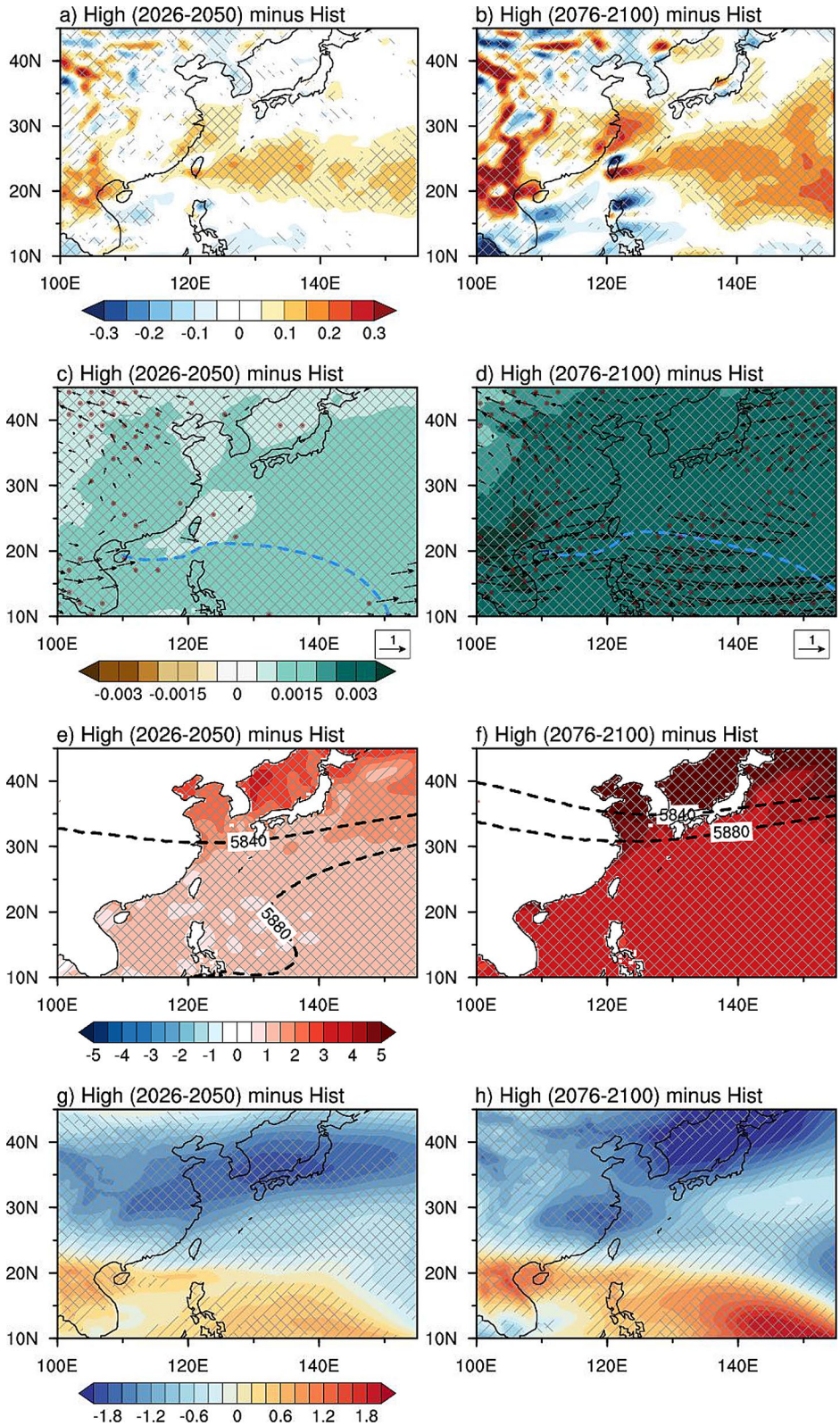

Fig. 11 (**a-b**) Relative vorticity at 850 hPa (10^{-5} s^{-1}); (**c-d**) specific humidity (shading, kg kg^{-1}), wind (vectors, m s^{-1}) at 850 hPa, and the monsoon trough (blue dashed line); (**e-f**) sea surface temperature (K) and geopotential height at 500 hPa with 5840 and 5880 gpm (black dashed lines); and (**g-h**) vertical wind shear (m s^{-1}) from June to November. Panels depict the differences between the high-emission scenario for the (left) near future (2026–2050) and (right) far future (2076–2100) relative to the historical period (1981–2005). Slashes indicate significance at the 90% confidence level based on the Student's t-test. The vectors are shown only in regions that are statistically significant. Backslashes represent consistency across RCMs, where 10 RCMs exhibit the same signal. Red dots indicate locations where such signals are evident in the vectors. Hatched lines represent regions meeting both criteria

periods simulated positive relative vorticity above 20 °N, with a stronger and more widespread in the MT (Fig. 11b). This distribution could lead to increased TCs near the ECS in the near future and over the MT in the far future (Fig. 8a and b). The difference between the two future periods and the historical period indicated an increase in the amount of water vapor across the domain in the near future, with a larger increase in the far future period (Fig. 11c and d). The low-level wind showed an enhanced westerly below 20 °N in the future period, but this was not statistically significant. The enhancement was more pronounced in the far future period, where cyclonic circulation emerged, contributing to increased positive relative vorticity and monsoon trough over MT (see Fig. 11b). The difference between future scenarios and historical experiments indicated an SST increase in both the near and far future periods, particularly towards the mid-latitude rather than the low-latitude (Fig. 11e and f). Moreover, the magnitude of SST increase was greater in the far future. This pronounced warming in the far future could allow the air masses to contain more water vapor, contributing to more vigorous TC intensity despite a shorter duration in the near future (Table 3). Furthermore, this SST increase leads to a decrease in the meridional temperature gradient, which affects upper-level jet distribution at mid-latitude according to the thermal wind relationship. Consequently, the differences between the future and historical periods showed a weaker VWS at mid-latitude, which was more noticeable in the far future (Fig. 11g and h). Moreover, TC activity might increase from the south of Japan in the near future to the Korean Peninsula because WNPSH has been shifted northwestward compared to the historical period. In the far future, the WNPSH has expanded northwestward compared to the near future period, which could suggest a decrease in TC activity below 30 °N. Additionally, to comprehend the causes of the decrease in TC occurrences at low-latitude, we analyzed the meridional mean wind field (10 °N −20 °N) using forcing data (not shown). The location of upward motion had shifted eastward in the future periods due to changes in the zonal circulation. This resulted in a larger difference in upper and lower wind direction and speed, intensifying VWS compared to the historical period. This strengthened VWS suppressed the development of low-latitude TCs.

In short, stronger low-level westerly anomalies between 10 °N −20 °N were expected to increase VWS, reducing TC frequency and activity in future periods. Conversely, these lower-level wind field changes induced positive relative vorticity at mid-latitude, potentially enhancing TC development. Increased mid-latitude SST weakened the mid-latitude jet and VWS, possibly increasing mid-latitude TC activity in the near future. Although TC frequency might decline in the far future, stronger TCs were anticipated, potentially causing greater damage upon landfall in East Asia.

5 Summary and conclusion

In this study, we investigated future projections of TCs under the high emission scenarios using CORDEX-EA phase 2 RCMs (HadGEM3-RA, CCLM, MM5, GRIMs, RegCM4.0 and 4.6, and WRF) forced by combinations of three GCMs through the ensemble method. We assessed the TC simulations from 13 RCMs during the historical period and observed notable variations among them. The 13 RCMs effectively captured the core region of TC genesis as observed in the RSMC best track data.

The ENS of these 13 RCMs simulated a higher frequency of TCs in the SCS and a lower frequency in the PS compared to the RSMC best track data, resulting in reduced TC activity towards the Korean Peninsula and Japan. The mean NTC was similar to observation, but they exhibited lower intensity and shorter duration compared to the historical period. The RCMs tended to simulate core regions larger than observations, but under-simulating strong TCs (TY category) on average. This underestimation may be attributed to the coarse resolution of RCMs. The weakening anticyclonic circulation in the SCS and WNP contributed to a positive relative vorticity bias, increasing TC occurrences. Conversely, the cyclonic circulation bias in WNP led to reduced TC activity in the ECS. In addition, negative SST and positive VWS biases created an unfavorable environment for TC maintenance. Despite these systematic biases, the spatial distributions of TC genesis and track densities were realistically reproduced in historical simulations.

TC activity under high emission scenarios was analyzed for both the near and far future. Results indicated an increase in TC activity south of Japan and the Korean Peninsula (10 °N −20 °N) in the near future, while the mean NTC decreased, and intensity did not change dramatically. In the far future, TC activity significantly decreased below 30 °N but increased over MT, with fewer NTC but stronger TCs. Both future periods showed a reduced frequency of the TS and STS categories TCs, whereas the TY category TCs were simulated more frequently on average, with the maximum value in the far future exceeding that of the near future period. The mean number of landfalling TCs was lower than in the historical period, although the MWS at landfall increased, especially in the far future. TCs with wind speeds exceeding the 70th percentile notably increased for the far future scenario above 25 °N, indicating potential significant impacts on the EA region. The changes in TC activity were linked to environmental factors: in the near future, the decrease (increase) in TC occurrence and activity

at low-latitude (mid-latitude) was attributed to stronger (weaker) VWS. The far future exhibited a similar pattern, while the relative vorticity and monsoon trough were strengthened, and WNPSH extended over the MT in the far future. Although both future periods had favorable conditions such as moistened air and warmer SSTs, these were more pronounced in the far future, contributing to higher intensity despite shorter durations.

In contrast to previous studies that investigated the future changes in TC activity in the EA region using a single GCM, RCM, or scenario, this study examined the future changes in TC activity simulated under the RCP8.5 and SSP5-8.5 scenarios, employing 13 RCMs with a 25-km horizontal resolution, forced by three GCMs. By employing a multi GCM-RCM chain, we aim to reduce uncertainty in TC projection for CORDEX-EA domain. Additionally, we emphasized that under future high-emission scenarios, the intensity of TCs making landfall in densely populated EA countries may increase, indicating a need for preparedness. This result could serve as a valuable reference for policymakers in addressing future climate change impacts and developing response strategies across various sectors.

However, increasing horizontal resolution is essential for a more realistic simulation of TC activities. The current 25-km horizontal resolution remains insufficient for accurately simulating the structure of TC core. Therefore, using RCMs with higher resolutions to simulate climate change may enable more precise representations of TC structure, intensity, and landfall. This, in turn, could facilitate a more detailed analysis of the surface wind profile, TC size, and the wind-pressure relationship, which could be effectively performed and presented with finer temporal intervals. Additionally, we used only high emission scenarios; future research will investigate TC activity under both low and high-emission scenarios. The differences between the RCP and SSP scenarios will also be analyzed.

Acknowledgments This work was funded by the Korea Meteorological Administration Research and Development Program under Grant (RS-2024-00403386). The model simulations were performed by using the supercomputing resource of the Korea Meteorological Administration (National Center for Meteorological Supercomputer).

Author contributions The authors confirmed contribution to the paper as follows: study conception and design: Eunji Kim, and Dong-Hyun Cha; data production and collection: Eunji Kim, Seok-Woo Shin, Dong-Hyun Cha, Eun-Chul Chang, Joong-Bae Ahn, Seung-Ki Min, Jin-Uk Kim, and Young-Hwa Byun; analysis and interpretation of results: Eunji Kim, Taehyung Kim, Taeho Mun, Minkyu Lee, and Dong-Hyun Cha; write manuscript text: Eunji Kim, and Dong-Hyun Cha; prepared figures: Eunji Kim. All authors reviewed the manuscript.

Funding Open Access funding enabled and organized by Ulsan National Institute of Science and Technology (UNIST).

Data availability RSMC best track data can be acquired from the Regional Specialized Meteorological Center (RSMC) Tokyo - Typhoon Center website (https://www.jma.go.jp/jma/jma-eng/jma-center/rsmc-hp-pub-eg/trackarchives.html). ERA5 data can be downloaded from the ECMWF website (https://www.ecmwf.int/en/forecasts/datasets/reanalysis-datasets/era5). Data used in this study can be provided upon request to the corresponding author.

Declarations

Conflict of interest All authors declare no conflict of interest.

References

Allen M, Pall P, Stone D, Stott P (2006) Scientific challenges in the attribution of harm to human influence on climate. U Pa L Rev 155:1353

Bacmeister JT, Reed KA, Hannay C, Lawrence P, Bates S, Truesdale JE, Rosenbloom N, Levy M (2018) Projected changes in tropical cyclone activity under future warming scenarios using a high-resolution climate model. Clim Change 146(3):547–560

Baek HJ, Lee J, Lee HS, Hyun YK, Cho C, Kwon WT, Marzin C, Gan SY, Kim MJ, Choi DH, Lee J, Lee J, Boo KO, Kang HS, Byun YH (2013) Climate change in the 21st century simulated by HadGEM2-AO under representative concentration pathways. Asia-Pac J Atmos Sci 49:603–618

Bell SS, Chand SS, Camargo SJ, Tory KJ, Turville C, Ye H (2019) Western North Pacific tropical cyclone tracks in CMIP5 models: statistical assessment using a model-independent detection and tracking scheme. J Clim 32(21):7191–7208

Bender MA, Knutson TR, Tuleya RE, Sirutis JJ, Vecchi GA, Garner ST, Held IM (2010) Modeled impact of anthropogenic warming on the frequency of intense Atlantic hurricanes. Science 327(5964):454–458

Cha DH, Jin CS, Lee DK, Kuo YH (2011) Impact of intermittent spectral nudging on regional climate simulation using Weather Research and forecasting model. J Geophys Research: Atmos, 116(D10).

Cha DH, Jin CS, Moon J, Lee DK (2016) Improvement of regional climate simulation of east Asian summer monsoon by coupled air-sea interaction and large-scale nudging. Int J Climatol 36:334–345

Chang P, Zhang S, Danabasoglu G, Yeager SG, Fu H, Wang H et al (2020) An unprecedented set of high-resolution earth system simulations for understanding multiscale interactions in climate variability and change. J Adv Model Earth Syst 12(12):e2020MS002298

Choi D, Kasdan DO, Yoon DK (2019) Analyzing disaster loss trends: a comparison of normalization methodologies in South Korea. Risk Anal 39(4):859–870

Coumou D, Rahmstorf S (2012) A decade of weather extremes. Nat Clim Change 2(7):491–496

Eyring V, Bony S, Meehl GA, Senior CA, Stevens B, Stouffer RJ, Taylor KE (2016) Overview of the coupled model Intercomparison Project Phase 6 (CMIP6) experimental design and organization. Geosci Model Dev 9(5):1937–1958

Fu ZH, Zhan R, Zhao J, Yamada Y, Song K (2023) Future projections of multiple Tropical Cyclone events in the Northern Hemisphere in the CMIP6-HighResMIP models. Geophys Res Lett 50(13):e2023GL103064

Gao X, Shi Y, Zhang D, Wu J, Giorgi F, Ji Z, Wang Y (2012) Uncertainties in monsoon precipitation projections over China: results from two high-resolution RCM simulations. Climate Res 52:213–226

Gao XJ, Wu J, Shi Y, Wu J, Han ZY, Zhang DF et al (2018) Future changes of thermal comfort conditions over China based on multi-RegCM4 simulations. Atmospheric Ocean Sci Lett 11(4):291–299

Giorgetta MA, Jungclaus J, Reick CH, Legutke S, Bader J, Böttinger M et al (2013) Climate and carbon cycle changes from 1850 to 2100 in MPI-ESM simulations for the coupled model Intercomparison Project phase 5. J Adv Model Earth Syst 5(3):572–597

Giorgi F, Gutowski Jr WJ (2015) Regional dynamical downscaling and the CORDEX initiative. Annu Rev Environ Resour 40:467–490

Giorgi F, Jones C, Asrar GR (2009) Addressing climate information needs at the regional level: the CORDEX framework. World Meteorological Organ (WMO) Bull 58(3):175

Giorgi F, Coppola E, Jacob D, Teichmann C, Omar A, Ashfaq S, M. et al (2022) The CORDEX-CORE EXP-I initiative: description and highlight results from the initial analysis. Bull Am Meteorol Soc 103(2):E293–E310

He C, Zhou T, Lin A, Wu B, Gu D, Li C, Zheng B (2015) Enhanced or weakened western North Pacific subtropical high under global warming? Sci Rep 5(1):16771

Hersbach H, Bell B, Berrisford P, Hirahara S, Horányi A, Muñoz-Sabater J et al (2020) The ERA5 global reanalysis. Q J R Meteorol Soc 146(730):1999–2049

Hong CC, Tsou CH, Hsu PC, Chen KC, Liang HC, Hsu HH et al (2021) Future changes in tropical cyclone intensity and frequency over the western North Pacific based on 20-km HiRAM and MRI models. J Clim 34(6):2235–2251

Huang WR, Chan JC (2014) Dynamical downscaling forecasts of Western North Pacific tropical cyclone genesis and landfall. Clim Dyn 42:2227–2237

IPCC (2021) In: Masson-Delmotte V, Zhai P, Pirani A, Connors SL, Péan C, Berger S, Caud N, Chen Y, Goldfarb L, Gomis MI, Huang M et al (eds) Climate Change 2021: the physical science basis. Contribution of Working Group I to the Sixth Assessment Report of the Intergovernmental Panel on Climate Change. Cambridge University Press, Cambridge, UK and NY

Jin CS, Cha DH, Lee DK, Suh MS, Hong SY, Kang HS, Ho CH (2016) Evaluation of climatological tropical cyclone activity over the western North Pacific in the CORDEX-East Asia multi-RCM simulations. Clim Dyn 47:765–778

Kim H-S, Ho C-H, Kim J-H, Chu P-S (2012) Track-pattern-based model for seasonal prediction of tropical cyclone activity in the western North Pacific. J Clim 25:4660–4678

Kim KB, Lee EH, Seol KH (2017) Sensitivity of typhoon simulation to physics parameterizations in the global model. Atmosphere 27(1):17–28 (in Korean)

Kim JM, Son S, Lee S, Son K (2020) Cost of climate change: risk of building loss from typhoon in South Korea. Sustainability 12(17):7107

Kim DH, Kim JU, Byun YH, Kim TJ, Kim JW, Kim YH et al (2021a) Future projection of extreme climate over the Korean Peninsula using Multi-RCM in CORDEX-EA phase 2 project. Atmosphere 31(5):607–623 (in Korean)

Kim G, Cha DH, Park C, Jin CS, Lee DK, Suh MS et al (2021b) Evaluation and projection of regional climate over East Asia in CORDEX-East Asia Phase I experiment. Asia-Pac J Atmos Sci 57:119–134

Kim K, Yoon D, Cha DH, Im J (2023a) Improved Tropical Cyclone Track Simulation over the Western North Pacific using the WRF Model and a machine learning method. Asia-Pac J Atmos Sci 59(3):283–296

Kim T, Kim E, Lee M, Cha DH, Lee SM, Lee J, Boo KO (2023b) Characteristics of tropical cyclones over the western North Pacific related to extreme ENSO and a climate regime shift in sub-seasonal forecasting with GloSea5. Clim Dyn 61(5):2637–2653

Kim YH, Ahn JB, Suh MS, Cha DH, Chang EC, Min SK et al (2023c) Future changes in extreme heatwaves in terms of intensity and duration over the CORDEX-East Asia Phase two domain using multi-GCM and multi-RCM chains. Environ Res Lett 18(3):034007

Knutson TR, Sirutis JJ, Garner ST, Vecchi GA, Held IM (2008) Simulated reduction in Atlantic hurricane frequency under twenty-first-century warming conditions. Nat Geosci 1(6):359–364

Lagare MC, Coronel R, Cruz F, Narisma GT, Villafuerte M, Tibay J (2022) Impacts of planetary boundary layer parameterization in RegCM4. 7 on the intensity and structure of simulated tropical cyclones over the Philippines. Clim Dyn 59(9–10):2915–2928

Lee JW, Hong SY (2014) Potential for added value to downscaled climate extremes over Korea by increased resolution of a regional climate model. Theoret Appl Climatol 117:667–677

Lee H, Jin CS, Cha DH, Lee M, Lee DK, Suh MS et al (2019) Future change in tropical cyclone activity over the western North Pacific in CORDEX-East Asia multi-RCMs forced by HadGEM2-AO. J Clim 32(16):5053–5067

Lee M, Cha DH, Suh MS, Chang EC, Ahn JB, Min SK, Byun YH (2020) Comparison of tropical cyclone activities over the western North Pacific in CORDEX-East Asia phase I and II experiments. J Clim 33(24):10593–10607

Li RC, Zhou W, Shun CM, Lee TC (2017) Change in destructiveness of landfalling tropical cyclones over China in recent decades. J Clim 30(9):3367–3379

Li J, Bao Q, Liu Y, Wang L, Yang J, Wu G et al (2021) Effect of horizontal resolution on the simulation of tropical cyclones in the Chinese academy of sciences FGOALS-f3 climate system model. Geosci Model Dev 14(10):6113-6133

Manganello JV, Hodges KI, Kinter III, Cash JL, Marx BA, Jung L, T. et al (2012) Tropical cyclone climatology in a 10-km global atmospheric GCM: toward weather-resolving climate modeling. J Clim 25(11):3867–3893

Moon J, Cha DH, Lee M, Kim J (2018) Impact of spectral nudging on real-time tropical cyclone forecast. J Geophys Research: Atmos 123(22):12–647

Mun T, Park H, Cha DH, Song CK, Min SK, Son SW (2024) Did recent sea surface temperature warming reinforce the extreme east Asian summer monsoon precipitation in 2020? Weather Clim Extremes 44:100682

Murakami H, Wang B (2010) Future change of North Atlantic tropical cyclone tracks: projection by a 20-km-mesh global atmospheric model. J Clim 23(10):2699–2721

Oh SG, Suh MS, Cha DH (2013) Impact of lateral boundary conditions on precipitation and temperature extremes over South Korea in the CORDEX regional climate simulation using RegCM4. Asia-Pac J Atmos Sci 49:497–509

Otto FE, Van Oldenborgh GJ, Eden J, Stott PA, Karoly DJ, Allen MR (2016) The attribution question. Nat Clim Change 6(9):813–816

Park DSR, Ho CH, Nam CC, Kim HS (2015) Evidence of reduced vulnerability to tropical cyclones in the Republic of Korea. Environ Res Lett 10(5):054003

Park C, Min SK, Lee D, Cha DH, Suh MS, Kang HS et al (2016) Evaluation of multiple regional climate models for summer climate extremes over East Asia. Clim Dyn 46:2469–2486

Roberts MJ, Camp J, Seddon J, Vidale PL, Hodges K, Vannière B et al (2020a) Projected future changes in tropical cyclones using the CMIP6 HighResMIP multi-model ensemble. Geophys Res Lett 47(14):e2020GL088662

Roberts MJ, Camp J, Seddon J, Vidale PL, Hodges K, Vanniere B et al (2020b) Impact of model resolution on tropical cyclone simulation using the HighResMIP–PRIMAVERA multimodel ensemble. J Clim 33(7):2557–2583

Sellar AA, Jones CG, Mulcahy JP, Tang Y, Yool A, Wiltshire A et al (2019) UKESM1: description and evaluation of the UK Earth System Model. J Adv Model Earth Syst 11(12):4513–4558

Seo GY, Ahn JB, Cha DH, Suh MS, Min SK, Chang EC et al (2023) Evaluation of multi-RCM ensembles for simulating spatiotemporal variability of Asian summer monsoon precipitation in the CORDEX-East Asia phase 2 domain. Int J Climatol 43(8):3710–3729

Shen W, Tang J, Wang Y, Wang S, Niu X (2017) Evaluation of WRF model simulations of tropical cyclones in the western North Pacific over the CORDEX East Asia domain. Clim Dyn 48:2419–2435

Stott PA, Christidis N, Otto FE, Sun Y, Vanderlinden JP, van Oldenborgh GJ et al (2016) Attribution of extreme weather and climate-related events. Wiley Interdisciplinary Reviews: Clim Change 7(1):23–41

Strachan J, Vidale PL, Hodges K, Roberts M, Demory ME (2013) Investigating global tropical cyclone activity with a hierarchy of AGCMs: the role of model resolution. J Clim 26(1):133–152

Suh MS, Oh SG, Lee DK, Cha DH, Choi SJ, Jin CS, Hong SY (2012) Development of new ensemble methods based on the performance skills of regional climate models over South Korea. J Clim 25(20):7067–7082

Taylor KE, Stouffer RJ, Meehl GA (2012) An overview of CMIP5 and the experiment design. Bull Am Meteorol Soc 93(4):485–498

Tong Y, Gao X, Xu Y, Cui X, Giorgi F (2024) Inter-comparison of precipitation simulation and future projections over China from an ensemble of multi-GCM driven RCM simulations. J Geophys Research: Atmos, 129(7), e2023JD040166.

Torres-Alavez JA, Glazer R, Giorgi F, Coppola E, Gao X, Hodges KI et al (2021) Future projections in tropical cyclone activity over multiple CORDEX domains from RegCM4 CORDEX-CORE simulations. Clim Dyn 57:1507–1531

Tran TL, Ritchie EA, Perkins-Kirkpatrick SE, Bui H, Luong TM (2022) Future changes in tropical cyclone exposure and impacts in Southeast Asia from CMIP6 pseudo-global warming simulations. Earth's Future, 10(12):e2022EF003118

von Storch H, Langenberg H, Feser F (2000) A spectral nudging technique for dynamical downscaling purposes. Mon Weather Rev 128(10):3664–3673

Wang Y, Wen S, Li X, Thomas F, Su B, Wang R, Jiang T (2016) Spatiotemporal distributions of influential tropical cyclones and associated economic losses in China in 1984–2015. Nat Hazards 84:2009–2030

Wu J, Gao X, Zhu Y, Shi Y, Giorgi F (2022) Projection of the future changes in tropical cyclone activity affecting East Asia over the western North Pacific based on multi-RegCM4 simulations. Adv Atmos Sci 39(2):284–303

Xi D, Chu K, Tan ZM, Gu JF, Shen W, Zhang Y, Tang J (2021) Characteristics of warm cores of tropical cyclones in a 25-km-mesh regional climate simulation over CORDEX East Asia domain. Clim Dyn 57:2375–2389

Yoon D, Cha DH, Lee G, Park C, Lee MI, Min KH (2018) Impacts of synoptic and local factors on heat wave events over southeastern region of Korea in 2015. J Geophys Research: Atmos 123(21):12–081

Zou L, Qian Y, Zhou T, Yang B (2014) Parameter tuning and calibration of RegCM3 with MIT–Emanuel cumulus parameterization scheme over CORDEX East Asia domain. J Clim 27(20):7687–7701